3rd International Symposium on Fatigue Design and Material Defects, FDMD 2017, 19-22 September 2017, Lecco, Italy

Strain concentrations in BCC micro lattices obtained by AM

L. Boniotti[*], S. Beretta, S. Foletti, L. Patriarca

Politecnico di Milano, Dept. Mechanical Engineering, Via La Masa 1, 20156 Milano, Italy

Abstract

The micro-lattices produced by additive manufacturing process (AM) represent a recent important advancement for engineering structural applications, in particular for weight-saving purposes. The design of the components manufactured with these meta-materials generally refers to the idealized structures. In reality, the geometry obtained by the AM process profoundly differs from the original one, in particular local geometrical irregularities were found to produce local stress and strain localizations which are difficult to be a-priori predicted by the analyses on the idealized structures. These geometrical defects may have a significant role for the structural integrity of the component and it is important to quantify their effect on the local stress and strain fields. In this study, we present an experimental investigation of a typical AlSi10Mg micro-lattice, namely the BCC cell. 3D tomography was used to reconstruct the original geometry and, successively, full-field digital image correlation strain measurements were performed to capture the localization of strains which are considered the precursor of the micro-lattice damage. The local strain measurements were used to calculate and classify the strain concentration factors arising from the geometrical irregularities. These results were compared with the finite element results obtained for the idealized and the real micro-lattice geometries providing important considerations for the structural integrity assessment of the components produced with the AM micro-lattices.

[*] Corresponding author. Tel.: +039 02 2399 8248.
E-mail address: laura.boniotti@polimi.it

1. Introduction

Nowadays, the additive manufacturing (AM) process enables the fabrication of complex geometric shapes, such as the lattice and the cellular structures, which imparts a profound improvement for manufacturing mechanical structures where the weight is a crucial design parameter, for example for the aerospace industry. The main advantage of using AM to produce lattice structures is the design flexibility, which is almost unconstrained from the manufacturing process [1]. Selective Laser Melting (SLM) is an AM technology capable of producing functional prototypes with complex geometries and thin structural walls. In SLM technology, the metallic powders are molten layer-by-layer by the laser energy to produce dense metal parts. Aluminum alloys have been found to be very attractive for manufacturing parts characterized by relatively good mechanical properties and a high strength to weight ratio [2]. The construction of small metallic parts with complex shapes and high resolution is feasible only using this process route [3]. Metallic micro-lattices consist of micro struts stacked in different arrangements where the volume fraction of the metal is much lower than the one of the metamaterial so obtained. Relative density and strut stacking are the prime design variables of this ultra-light material and the mechanical properties can be engineered by controlling these parameters [4]. For this reason, micro-lattice materials can be considered as a uniform material at the macroscale [5] while, at the microscale, the structure is detailed as formed by joined struts [6-7].

One of the most relevant problem is that the design of the components manufactured with these meta-materials generally refers to the idealized structures. In reality, the geometry obtained by the AM process profoundly differs from the original one [8-9-10], in particular local geometrical irregularities were found to produce stress and strain localizations, which are difficult to be a-priori predicted by analysing the idealized structures. All these defects can lead to the failure of the structure and, therefore, it is crucial to analyze the stress and strain concentrations inside the unit cells in order to improve the design of these microstructures.
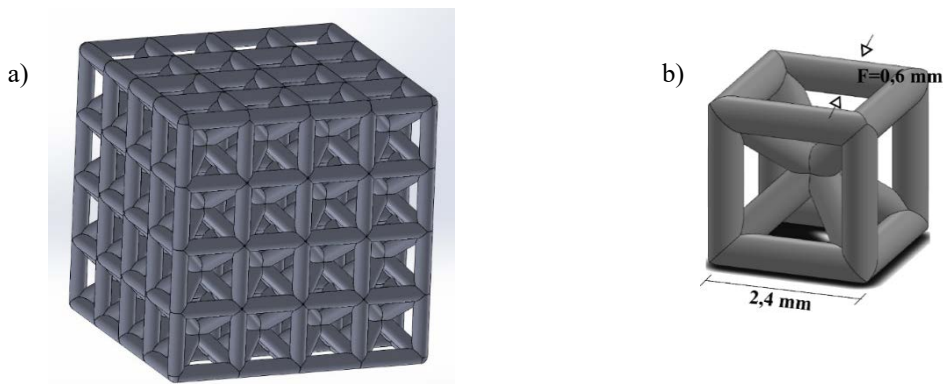

Figure 1. (a) Ideal geometry of the specimen; (b) BCC ideal unit cell. (aggiungere sistema di rif)

This work presents an experimental investigation of a typical AlSi10Mg micro-lattice, namely the BCC cell (Figure 1a, 1b). The 3D tomography [11] was used to reconstruct the original geometry for a detailed model of the lattice structure for the sake of analysis. Successively, full-field digital image correlation (DIC) strain measurements were performed during a compressive test to capture the localization of strains, which are considered the precursor of the micro-lattice damage. Then the geometrical defects were classified in three groups according to their origin and a strain concentration factor K_ε was introduced to quantify these localizations. The local strain measurements were used to calculate and classify the strain concentration factors arising from the geometrical irregularities.

The experimental results were compared with the elastic finite element (FE) results obtained for the idealized and real micro-lattice geometries providing important considerations for the structural integrity assessment of the components produced with the AM micro-lattices.

2. Experiments

2.1 Material and sample

The micro-lattice structure of the compressive sample is composed of BCC unit cells and it is manufactured with SLM of a pre-alloyed AlSi10Mg powder with average powder size of 30 μm. AlSi10Mg is a typical casting alloy and it can be used to produce cast parts with thin walls and complex geometry [12-13]. All struts have an ideal circular section with a diameter equal to 0.6 mm and a length of 2.4 mm (Figure 1b). The sample is cubic and is composed by 64 cells (Figure 1a). The real geometry of the printed sample profoundly differs from the ideal geometry (Figure 2). The cross section of the struts was found to be different than the expected circular shape [8]. In addition, the strut thickness is not regular: it changes along the strut axis and it is generally bigger than the idealized [9-10]. The external surface of this strut is irregular and multiple defects can be detected in the structure [14]. By means of micro-CT scans it is possible to see also internal pores in the material (figure 8c). Porosity, which is a common defect in metal additive manufacturing parts and can negatively affect mechanical properties of the material, was measured by means of micro-CT scans to be approximately 0.4%.
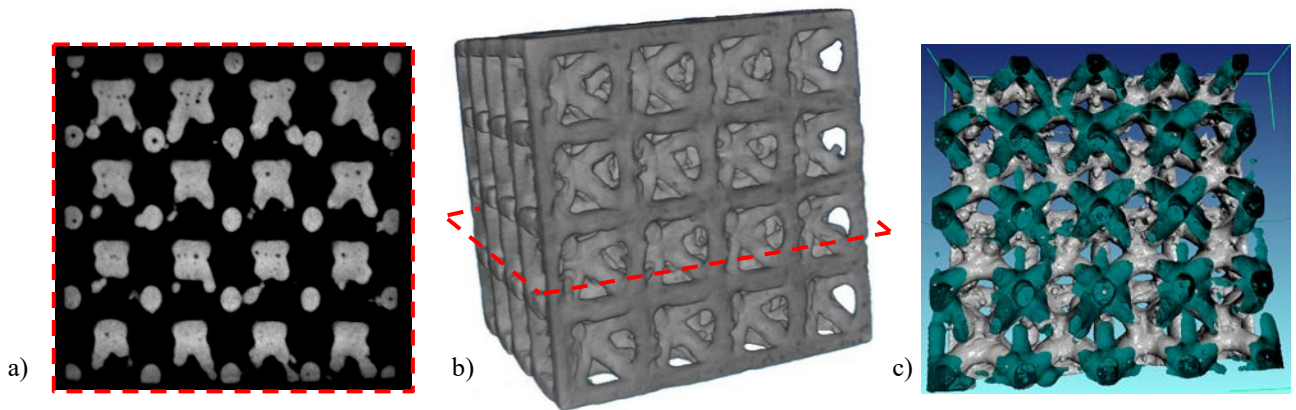

a)   b)   c)

Figure 2. (a) Section of the printed sample (micro tomography image); (b) Real geometry of the specimen (micro tomography reconstruction) (c) external surface and pores of the specimen (micro tomography surface).

2.2 Test setup

A compression test was performed under a MTS Alliance RF/150 testing machine in displacement control at a rate of 0.1mm/min (Figure 3). The test was stopped at nine different load steps and the maximum load reached was equal to 8.8 kN. A spherical joint was used to optimize the alignment between the loaded surface of the sample and the upper grip. In order to measure continuously the displacement during the test, a deflectometer was used according the schematic proposed in Figure 3b. This set-up enabled to measure the average axial strain of the sample during the test.

A speckle pattern was created in the front face of the specimen by means of an IWATA aerograph and an appropriate nitro black paint that was sprayed on the sample surface. During the test, multiple images of the target specimen surface were captured in order to increase the strain resolution and, at the same time, map the entire sample surface. In detail, the surface of the sample was virtually divided in six parts and, in every load step, six images were manually captured at a resolution of approximately 2.34μm/px. These images were successively stitched and correlated by a commercial software. Local and average strains in the sample were mapped and measured during the sample deformation.
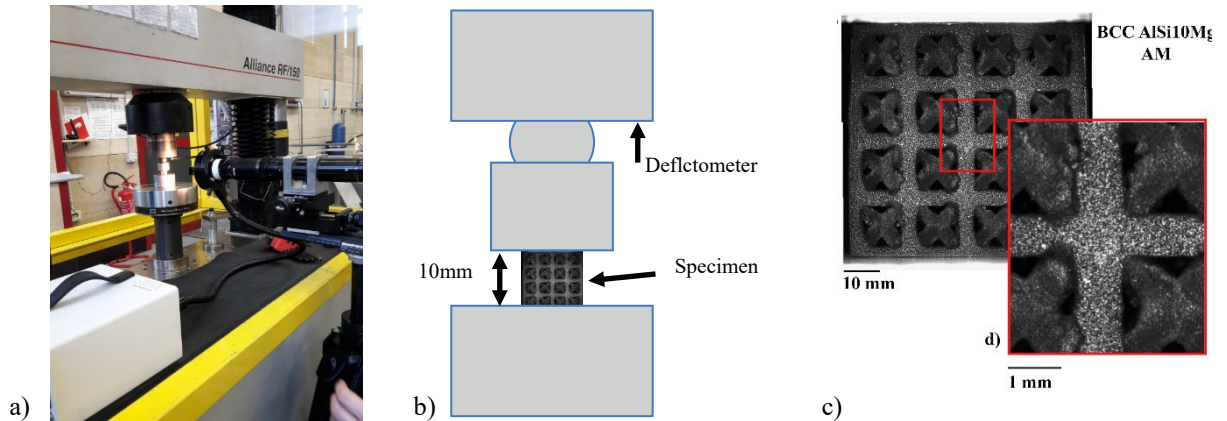
Figure 3. (a) Test machine and DIC camera; (b) Scheme of the experimental test; (c) Speckle pattern.

2.3 Test results

During the compressive test, nine interruptions have been performed: 0 kN (before starting the test), 2kN, 4kN, 5kN, 6kN, 7kN, 8.8kN, 0 kN (after the final unload). The stress-strain curve was determined using the displacements from the deflectometer (blue line in Figure 4) and the average strain measured on the DIC surface (orange line).

The curves slightly differ as the deflectometer was influenced by the elements interposed between the surface of the sample and the upper plate where it was positioned.
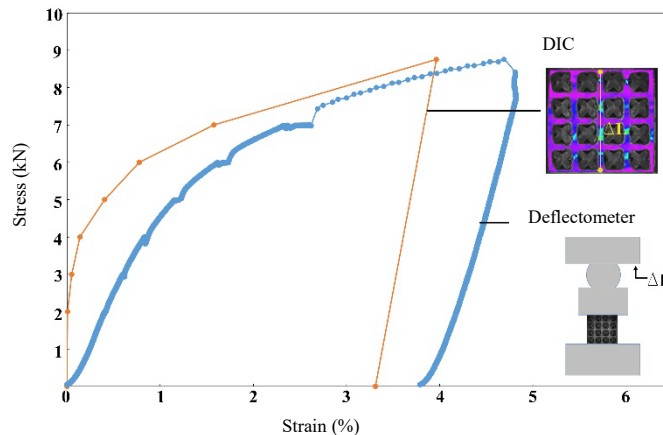

Figure 4. Stress-strain curves.

3. DIC analysis

3.1 Defects classification

Looking at the defects in the struts analyzed by the DIC, it is possible to observe that different types of imperfections in the geometry leaded to different strain concentrations in the microstructure. It is important to point out that, using an ideal geometry, it is not possible to predict these stress and strain concentrations. The defects have been classified in three different groups (Figure 5). The first type of defect is the variation of the strut cross-section. In some struts, parts with smaller diameters were observed. These geometrical discontinuities induced a decrease of the buckling load (Figure 5a). The second type of defects depends on the geometry of the cells: the conjunction of the struts corresponds to a geometrical notch, which promotes stress and strain localizations (Figure 5b). The last group

of defects are observed on the surface: the printing process can create a point with indentations or protrusions, with material in exceedance or lack of material (Figure 5c).

In reality, an appropriate speckle pattern is characterized by a plane and regular pattern. Therefore, it is necessary to create a flat surface of the sample. For this reason, by means of a polishing with abrasive papers, part of material of the struts on the surface was removed. As a result, in some location of the micro-lattice, the local buckling load was further decreased by specimen preparation. However, this effect was considered in the FE simulations as the 3D tomography was performed on the specimen after preparation and a proper comparison was obtained.

According to these preliminary observations, the real lattice structure has a mechanical behavior that differs from the behavior predicted by analyzing the ideal structure. In the case of an idealized geometry with regular struts, it is possible to study a strut as a built-in beam [15-16]. Indeed, in the case of a real geometry, strain and stress concentrations in the real structure are not negligible. They are very important to evaluate the static strength and the fatigue limit of micro-lattices.
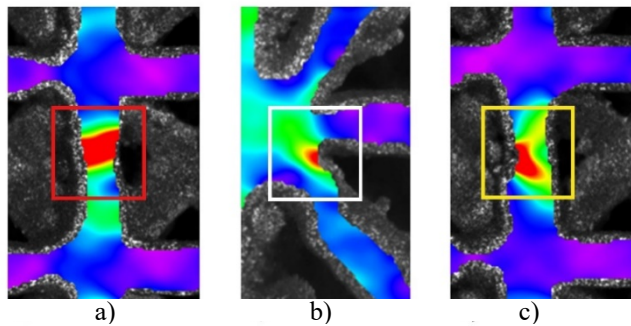

a)   b)   c)

Figure 5. (a) Buckling defect; (b) geometrical defect; (c) printing defect.

3.1 Local strain concentration

In order to estimate the strain concentration in the microstructure, a strain concentration factor K_ε was introduced. This factor is defined as the ratio between the maximum axial strain (in the load direction) adjacent to the defect and the average strain measured in the strut that contains the defect, as shown in Eq. 1.

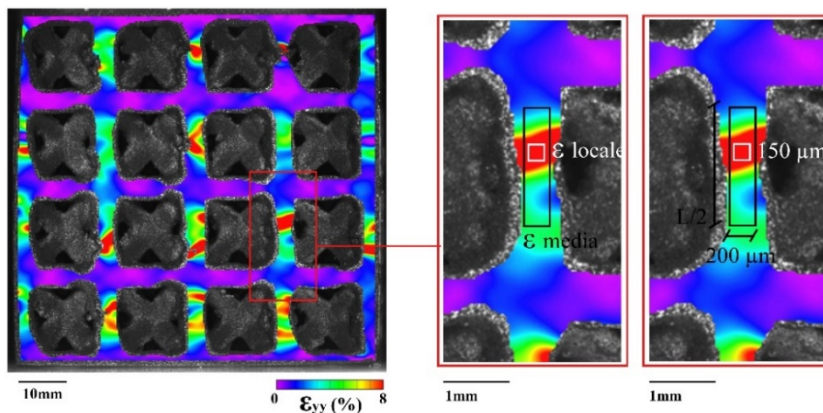$$K_\varepsilon = \frac{\varepsilon_{local}}{\varepsilon_{strut}} \tag{1}$$

Figure 6. Local and average strains measurement.

In detail, the local strain is obtained as the mean of the strain values in a square area of 150 μm x 150 μm, as shown in Figure 6. The size of this area was chosen according the Line Method and the El-Haddad parameter of the aluminum

[16-17]. The average strain is measured in an area of width equal to 200 μm and height of approximately L/2, where L is the strut length.

Figure 6 shows the classification of the defects in the sample: the red color indicates the buckling defects, while the yellow one the printing defects. There are no geometrical defects in this BCC structure. In fact, the analyzed external surface has a simple geometry, only with vertical and horizontal struts. This type of defect is in the intersections of the internal struts.

The K_ε factor was estimated at the load step at 6 kN. For this load step the plastic strains is very low. As it can be seen from Fig. 6, the adoption of a 'local' calculation of Ke is needed because the load is not uniform among the vertical struts.

4. Finite Element Analysis

After analyzing the experimental test and the DIC, the results were compared with FE analyses. The first model analyzed is based on an ideal geometry of the sample (Figure 7a). A total of 834434 quadratic elements were used to construct the idealized FE model. For this FE analysis, the struts are regular and low strain localizations were detected.
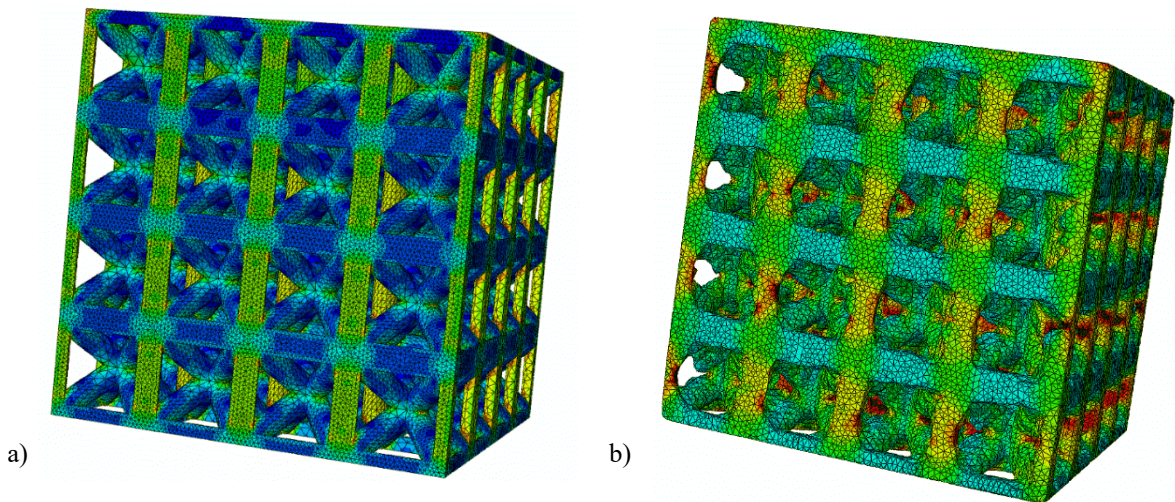

Figure 7. (a) FE model with ideal geometry; (b) DIC; (c) FE model with real geometry

The FE model of the real structure defined from the micro-tomography (Figure 7b), was then analyzed. The mesh of this real geometry was obtained by means of the open-source software Fiji and the plug-in Bonej [18]. A total of 3595450 four-node tetrahedral elements were generated for this FE model with an average dimension of 100μm on the external surface and around 40 μm inside the volume. In this case, in the FE model multiple strain concentrations were observed, in locations qualitatively similar to the strain concentrations measured with the DIC.

5. Results

5.1 *Results from DIC*

The K_ε factor was evaluated in every vertical strut. In Figure 8, the K_ε values are divided in two different groups based on the type of the defects that generate the strain concentration. For the strain localizations arising from the

printing defects we measured an average K_ε of 1.52, while for the buckling defects 1.48. In both cases, the maximum K_ε factor measured was 1.91 for the printing defects and the 2.02 for bucking defects.
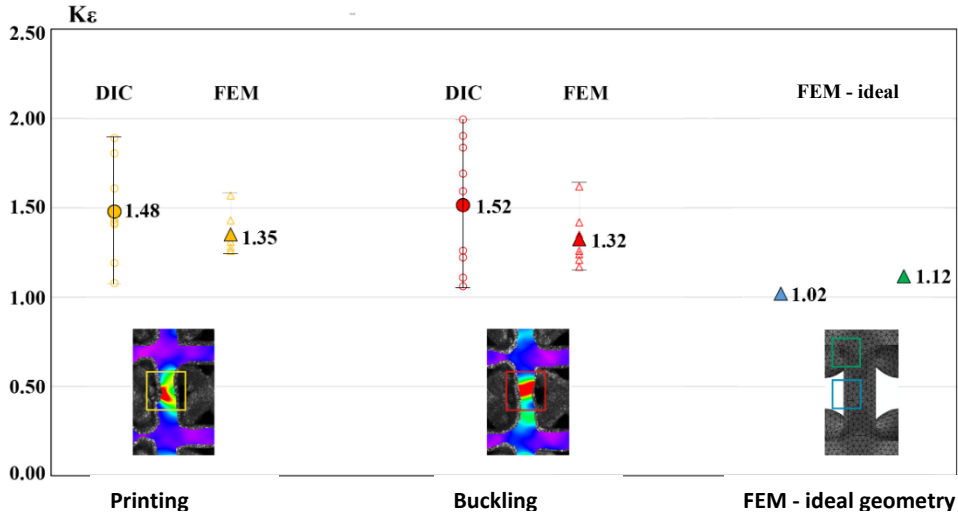

Figure 8. Strain concentration factor plot for the bcc micro-lattice geometry analyzed in this study.

5.1 *FEM results*

In the 3D FE model, it is possible to measure also strain localizations in the internal struts of the lattice structure and these localizations (geometrical defects at the joints of the cell) can also be higher than those on the external surface considered. However, in this work a comparison between DIC and FE results was neemed, so only strain localizations on the external surface were considered. Strain values were measured in terms of the Y-strain at the nodes of the elements of the external surface. The K_ε was measured as in the DIC as the ratio between local strain and average strain. Each local strain value was the mean of the strain values measured in the nodes of the elements contained in a square area of 150 μm x 150 μm adjacent to the defect on the external surface. The average strain for each vertical strut was measured as the mean of the strain values in the nodes of the elements contained in an area on the external surface of width equal to 200 μm and height of approximately L/2, where L is the strut length.

In the case of the real geometry strain localizations in the vertical struts were considered. For the idealized geometry, the K_ε was measured in the same way that in the DIC and in the real geometry model, referring to areas on the external surface with the same dimensions of the ones considered before. In this model there are no strain localizations in the vertical struts, so local strain and K_ε was measured in two positions. In the first case, K_ε was measured considering local strain in a square area in the middle of the vertical struts on the external surface. Then, K_ε was also measured considering local strain on a square area at the intersection between vertical and horizontal struts, where the model has strain concentrations. The results obtained are summarized in Figure 8. The first important consideration is that the FE model based on the real geometry is able to represent the mechanical behavior of the sample since strain localization occurs at the same regions where strain concentrations were observed in the experiments. The difference between experimental and numerical results is due to some limitations of the FE model. In fact, the computational burden of the geometrical reconstruction prevented, so far, to run a convergence analysis or to adopt a mesh with quadratic elements. In addition, the FE analysis on the real structure does not model the plastic behavior of the material which might be required to be considered since in the real structure local plastic strains arise even in the nominally elastic region of the stress-strain curve. The modelling of the plastic behavior will be considered for future developments.

6. Conclusions

This work presents an experimental investigation of a typical AlSi10Mg micro-lattices, namely the BCC cell, produced by SLM process. DIC strain measurements were performed during a compressive test to capture the localization of strains on the real cell. Successively, 3D tomography was used to reconstruct the original geometry and a FE model of the idealized and real structures were developed.

The main results from this activity are:

- significant strain concentrations were measured by DIC on the surface of samples made by BCC cells that were subjected to compressive tests;
- a first model was based on an ideal geometry of the sample derived from the design geometry: in this case struts are regular and very low strain localizations were detected
- a FE model based on the real geometry derived from the micro-tomography was analyzed. In this model multiple strain concentrations were observed to be qualitatively similar (although lower) to the strain concentrations measured with DIC.

The conclusion that can be presently drawn is that a model based on an ideal geometry does not permits to describe the real behavior of the printed lattice structure. Therefore estimates of the strength (both for static and fatigue loads) from a simplified geometry will likely be not precise enough for engineering calculations.

Acknowledgement

References

[1] Park S.I., Rosen D.W., Choi S.K., Duty C.E., Effective mechanical properties of lattice material fabricated by material extrusion additive manufacturing, *Additive Manufacturing*, Volumes 1–4, October 2014, Pages 12–23.

[2] Bartkowiak K., Ullrich S., Frick T., Schmidt M., New Developments of Laser Processing Aluminum Alloys via Additive Manufacturing Technique, *Physics Procedia*, Volume 12, Part A, 2011, Pages 393–401.

[3] Brandl E., Heckenberger U., Holzinger V., Buchbinder D., Additive manufactured AlSi10Mg samples using Selective Laser Melting (SLM): Microstructure, high cycle fatigue, and fracture behavior, *Mater. Des.*, vol. 34, pp. 159–169, 2012.

[4] Rashed M.G., Ashraf M., Mines R.A.W., Hazell P.J., Metallic microlattice materials: A current state of the art on manufacturing, mechanical properties and applications, (2016), doi: 10.1016/j.matdes.2016.01.146.

[5] Ashby M., Materials Selection in Mechanical Design (3rd ed.). Burlington, Massachusetts: Butterworth-Heinemann, 1999.

[6] Arabnejad Khanoki S., Pasini D., Mechanical properties of lattice materials via asymptotic homogenization and comparison with alternative homogenization methods, *International Journal of Mechanical Sciences*, 77 (2013), 249–262.

[7] Arabnejad Khanoki S., Pasini D., Multiscale design and multiobjective optimization of orthopedic hip implants with functionally graded cellular material, *Journal of Biomechanical Engineering*, march 2012, Vol. 134.

[8] Arabnejad Khanoki S., Johnston R.B., Pura J.A., Singh B., Tanzer M., Pasini D., High-strength porous biomaterials for bone replacement: A strategy to assess the interplay between cell morphology, mechanical properties, bone ingrowth and manufacturing constraints, *Acta Biomaterialia* 30 (2016) 345–356.

[9] Sutcliffe C., Brooks W., Cantwell W., Fox P., Todd J., and Mines R.A.W.,The rapid manufacture of micro hierarchical structures by selective laser melting. Proc. ICALEO 2005,Univ. of Liverpool, 2005.

[10] Tsopanos S., Mines R.A.W., McKown S., Cantwell W.J., Shen Y., Brooks W., The influence of processing parameters on the mechanical properties of selectively laser melted stainless steel microlattice structures. *J. Manuf. Sci. Eng.* 132, 2010.

[11] ASTM E1441-11, Standard Guide for Computed Tomography (CT) Imaging, 2011.

[12] Material data sheet, EOS Aluminium AlSi10Mg for EOSINT M 270, EOS GmbH, Vol. 90110024, 2011.

[13] Mazur M., Leary M., McMillan M., Sun S., Shidid D., Brandt M., Mechanical Properties of Ti6Al4V and AlSi12Mg. Lattice Structures Manufactured by Selective Laser Melting (SLM). *Laser Additive Manufacturing* 119 (2016).

[14] Rehme O., Emmelmann C. Rapid manufacturing of lattice structures with selective laser melting. Proceedings of the SPIE, Vol. 6107, 2006.

[15] Van Hooreweder B., Kruth J., Advanced fatigue analysis of metal lattice structures produced by Selective Laser Melting, *CIRP Annals - Manufacturing Technology*, 66 (2017) 221–224.

[16] De Krijger J., Rans C., Van Hooreweder B., Lietaert K., Pouran B., Zadpoor A., Effects of applied stress ratio on the fatigue behavior of additively manufactured porous biomaterials under compressive loading, *Journal of the mechanical behavior of biomedical materials*, 70 (2017)

[17] Romano S., Brandão A., Gumpinger J., Gschweitl M., Beretta S., "Qualification of AM parts: Extreme value statistics applied to tomographic Measurements", *Materials & Design*, 131 (2017) 32–48.

[18] Ferreira T., Rasband W., ImageJ User Guide, 2012.